UC Irvine
UC Irvine Previously Published Works

Title
The land–atmosphere water flux in the tropics

Permalink
https://escholarship.org/uc/item/7tc151h4

Journal
Global Change Biology, 15(11)

ISSN
1354-1013

Authors
FISHER, JOSHUA B
MALHI, YADVINDER
BONAL, DAMIEN
et al.

Publication Date
2009

DOI
10.1111/j.1365-2486.2008.01813.x

Peer reviewed

The land–atmosphere water flux in the tropics

JOSHUA B. FISHER*, YADVINDER MALHI*, DAMIEN BONAL†, HUMBERTO R. DA ROCHA‡, ALESSANDRO C. DE ARAÚJO§, MINORU GAMO¶, MICHAEL L. GOULDEN∥, TAKASHI HIRANO**, ALFREDO R. HUETE††, HIROAKI KONDO¶, TOMO'OMI KUMAGAI‡‡, HENRY W. LOESCHER§§, SCOTT MILLER¶¶, ANTONIO D. NOBRE∥∥, YANN NOUVELLON***, STEVEN F. OBERBAUER†††, SAMREONG PANUTHAI‡‡‡, OLIVIER ROUPSARD***, SCOTT SALESKA§§§, KATSUNORI TANAKA¶¶¶, NOBUAKI TANAKA∥∥∥, KEVIN P. TU**** and CELSO VON RANDOW††††

*Environmental Change Institute, School of Geography and the Environment, Oxford University, Oxford OX1 3QY, UK, †Ecophysiologie Forestière, INRA Kourou – UMR Ecofog, BP 709, 97387 Kourou cedex, French Guiana, ‡Instituto de Astronomia, Geofísica e Ciências Atmosféricas, Universidade de São Paulo Rua do Matão 1226, Sao Paulo 05508-900, Brazil, §Instituto Nacional de Pesquisas da Amazônia, Manaus, Amazonas, Brazil, ¶National Institute of Advanced Industrial Science and Technology, Tsukuba, Ibaraki 305-8569, Japan, ∥Department of Earth System Science, University of California at Irvine, Irvine, CA 92697-3100, USA, **Graduate School of Agriculture, Hokkaido University, Sapporo 060-8589, Japan, ††Department of Soil, Water and Environmental Science, University of Arizona, Tucson, AZ 85721, USA, ‡‡Shiiba Research Forest, Kyushu University, Shiiba-son, Miyazaki 883-0402, Japan, §§Department of Forest Science, Oregon State University, Corvallis, OR, USA, ¶¶State University of New York at Albany, ASRC 251, Albany, NY 12203, USA, ∥∥Instituto Nacional de Pesquisas na Amazonia, São José dos Campos, Sao Paulo 12201-970, Brazil, ***CIRAD, Avenue d'Agropolis, 34398 Montpellier Cedex 5, France, †††Department of Biological Sciences, Florida International University, Miami, FL, USA, ‡‡‡National Park, Wildlife and Plant Conservation Department, Thailand, §§§Department of Ecology and Evolutionary Biology, University of Arizona, Tucson, AZ 85721, USA, ¶¶¶Frontier Research Center for Global Change, Japan Agency for Marine-Earth Science & Technology, Yokohama, Kanagawa 236-0001, Japan, ∥∥∥University Forest in Aichi, Graduate School of Agricultural and Life Sciences, The University of Tokyo, 11-44 Goizuka, Seto City, Aichi 489-0031, Japan, ****Department of Integrative Biology, University of California at Berkeley, Berkeley, CA 94709, USA, ††††Instituto Nacional de Pesquisas Espaciais, Cachoeira Paulista, SP 12630-000, Brazil

Abstract

Tropical vegetation is a major source of global land surface evapotranspiration, and can thus play a major role in global hydrological cycles and global atmospheric circulation. Accurate prediction of tropical evapotranspiration is critical to our understanding of these processes under changing climate. We examined the controls on evapotranspiration in tropical vegetation at 21 pan-tropical eddy covariance sites, conducted a comprehensive and systematic evaluation of 13 evapotranspiration models at these sites, and assessed the ability to scale up model estimates of evapotranspiration for the test region of Amazonia. Net radiation was the strongest determinant of evapotranspiration (mean evaporative fraction was 0.72) and explained 87% of the variance in monthly evapotranspiration across the sites. Vapor pressure deficit was the strongest residual predictor (14%), followed by normalized difference vegetation index (9%), precipitation (6%) and wind speed (4%). The radiation-based evapotranspiration models performed best overall for three reasons: (1) the vegetation was largely decoupled from atmospheric turbulent transfer (calculated from Ω decoupling factor), especially at the wetter sites; (2) the resistance-based models were hindered by difficulty in consistently characterizing canopy (and stomatal) resistance in the highly diverse vegetation; (3) the temperature-based models inadequately captured the variability in tropical evapotranspiration. We evaluated the potential to predict regional evapotranspiration for one test region: Amazonia. We estimated an Amazonia-wide evapotranspiration of 1370 mm yr^{-1}, but this value is dependent on assumptions about energy balance closure for the tropical eddy covariance sites; a lower value (1096 mm yr^{-1}) is considered in discussion on the use of flux data to validate and interpolate models.

Keywords: Amazon, eddy covariance, evaporation, evapotranspiration, ISLSCP-II, LBA, model, remote sensing, tropical

Received 22 October 2008; revised version received 22 October 2008 and accepted 27 October 2008

Correspondence: Joshua B. Fisher, tel. + 44 1865 285182, fax + 44 1865 275885, e-mail: joshbfisher@gmail.com

Introduction

Tropical forests and savannas are a major source of global land surface evapotranspiration (latent heat of evaporation or LE), and thus drivers of the global atmospheric circulation and hydrological cycle (Numaguti, 1993; Larson et al., 1999; Werth & Avissar, 2004). Moreover, tropical ecosystems are responsible for half of the global terrestrial gross primary production, contain 40% of the carbon in the terrestrial biosphere, and mediate 21% of total freshwater inflow to the world oceans through four tropical rivers alone – the Amazon, Orinoco, Magdalena, and Congo (Baumgartner & Reichel, 1975; Grace et al., 2001). Understanding the tropical LE response to changing climate is critical to understanding the stability of the tropics in the larger global system (Hulme & Viner, 1998; Cox et al., 2000).

Accurate prediction of tropical LE is hindered by two problems. First, current LE models are often site specific (e.g., for agricultural and temperate systems), may require extensive parameterization or, conversely, may be too simple, and often include assumptions that are not robust for tropical forests (Shuttleworth, 1988; Kelly & Randall, 2001). Second, there have been few long-term measurements of LE above tropical vegetation with which to validate models. This data gap has been filling recently with the advent of eddy covariance studies at a number of tropical forest sites worldwide (Hasler & Avissar, 2007).

To understand how different LE models might perform for the tropics, we need to understand first how LE is controlled in the tropics. Near the equator, LE is seasonally in phase with net radiation (R_n), but is less so away from the equator due to seasonal water stress (Hasler & Avissar, 2007). Various climatic parameters can exhibit characteristic seasonal variation that can in turn influence rates of LE: albedo, air temperature (T_a), vapor pressure deficit (VPD), and precipitation (PPT) may exhibit seasonality (Kumagai et al., 2005; Loescher et al., 2005); LE may be sensitive to interannual PPT variability (Vourlitis et al., 2002; Malhi & Wright, 2004; Loescher et al., 2005). The soil moisture status after rains may be more important than total PPT (Malhi et al., 2002). Forests can continue transpiring during dry periods by reducing leaf canopies or absorbing water from soil depths of more than 8 m (Nepstad et al., 1994; Costa & Foley, 1997). Some researchers have shown that R_n, VPD, aerodynamic conductance, and stomata control LE in the tropics, whereas others have found that LE is not sensitive to some of these drivers (Shuttleworth, 1989; Granier et al., 1996; Williams et al., 1998; Malhi et al., 2002; Sommer et al., 2002; Vourlitis et al., 2002; Kumagai et al., 2005; Loescher et al., 2005; Juárez et al., 2007). Variability in the strength of these drivers

may be linked to different degrees of canopy–atmosphere coupling (Jarvis & McNaughton, 1986).

The Penman–Monteith (1965) equation, which depends on R_n, T_a, VPD, wind speed (u), and bulk stomatal resistance of the canopy (r_c), has been applied for tropical systems (Williams et al., 1998; Bigelow, 2001; Werth & Avissar, 2004; Loescher et al., 2005). However, because of its reliance on r_c, and the relative complexity of multilayered vertical canopy profiles in the tropics, this equation can be difficult to apply in tropical forests. Additionally, r_c may be difficult to parameterize spatially given the high levels of species diversity in the tropics. The Priestley & Taylor (1972) equation, however, which depends only on R_n and T_a, has been used successfully for the tropics (Kumagai et al., 2005; Loescher et al., 2005; Schüttemeyer et al., 2007). Although it is easy to parameterize, it lacks any direct response of the vegetation. Most other LE models are derivations from the Penman–Monteith and Priestley–Taylor equations (see Materials and methods), though simple T_a-based regression models have been used for the tropics as well.

Our objectives in this paper are to

(i) examine the controls on LE in tropical vegetation by collating the widest pan-tropical dataset of eddy covariance studies analyzed to date (i.e., building upon Hasler & Avissar, 2007);
(ii) conduct a comprehensive and systematic evaluation of the ability of different LE models to capture the temporal variability of LE fluxes;
(iii) assess the ability to scale up model estimates of LE for one test region – Amazonia – and explore the caveats and limitations of such an estimate.

Materials and methods

Data: eddy covariance

The study sites included a wide range of tropical biome types in South America, South-East Asia, Africa and Oceania (Fig. 1 and Table 1). Eddy covariance flux measurements for these sites have been described extensively (Araújo et al., 2002; Carswell et al., 2002; Malhi et al., 2002; Toda et al., 2002; Saleska et al., 2003; Tanaka et al., 2003; da Rocha et al., 2004; Epron et al., 2004; Goulden et al., 2004; Kruijt et al., 2004; Sakai et al., 2004; von Randow et al., 2004; Loescher et al., 2005; Roupsard et al., 2006; Hirano et al., 2007; Bonal et al., in press; Huete et al., 2008), including many as part of the Large-Scale Biosphere Atmosphere Experiment in Amazonia (LBA) and AsiaFlux. Site S77 experienced disturbance from irrigation, harvesting, and burning during the measurement period and was excluded from summary statistics. Site BKS was excluded from energy
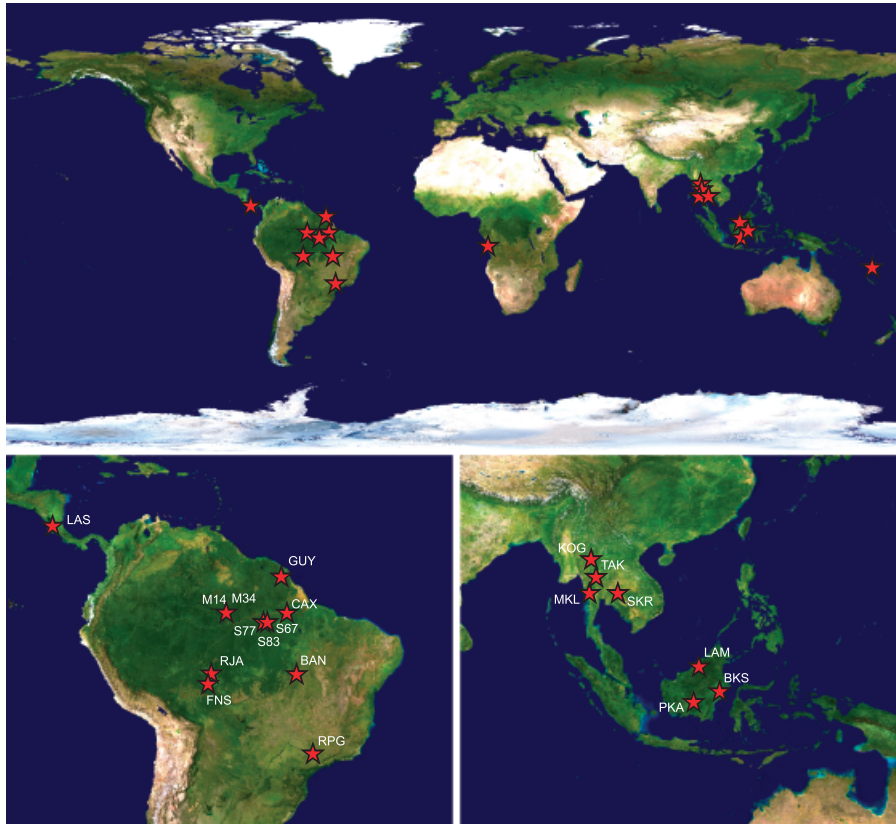
Fig. 1 Locations of the 21 tropical eddy covariance sites with insets to the Amazon and South-East Asia for detailed locations of the sites.

balance closure estimates due to severe energy balance mismatch. Meteorological measurements included in this analysis were R_n, VPD, T_a, u, and PPT. We defined VPD as the difference in water vapor content between 100% relative humidity (RH) at the air temperature near the leaves and the ambient specific humidity of the air at the above-canopy measurement point. Micrometeorological instruments were attached to towers extending above the site canopies. The eddy covariance method was used to quantify vertical fluxes of scalars (i.e., water vapor) between the ecosystem and the atmosphere from the covariance between vertical wind velocity and scalar fluctuations (Shuttleworth *et al.*, 1984; Baldocchi *et al.*, 2001).

Most tropical forests sites within the LBA are reporting energy balance closure[1] to within 70–80%, but the missing 20–30% is poorly understood due, in part, to footprint representation (Malhi *et al.*, 2002; Wilson *et al.*, 2002; Hasler & Avissar, 2007). Because flux measurements are often unreliable at night due to low and intermittent wind turbulence (Aubinet *et al.*, 2003; Fisher *et al.*, 2007), daytime measurements were used in this

[1]$(LE + H + G + S)/R_n = 1$, where H is the sensible heat flux, G is the soil heat flux, and S is the canopy storage flux.

analysis though closure increases slightly when night-time values are included (night-time LE is minimal, regardless), as the canopy storage flux approaches zero over periods greater than 24 h. Energy balance closure at the tropical forests sites in this analysis was 80% for monthly daytime averages (Fig. 2). Although the storage term (G) was not always available, on average it was less than 2% of total R_n. We used monthly averages based on averaging of half-hour (provided) to daily to monthly values. We excluded any given average if fewer than 75% of data time steps were available – for example, we would include a daily average if 18 of the 24 half-hourly values were not missing. We did not gap-fill with a model to avoid circularity with model testing.

Perhaps the most important question when comparing eddy covariance data against models of LE is how we treat the lack of energy balance closure. Does the lack of energy balance closure at eddy covariance sites indicate (i) 'missing' turbulent fluxes (both latent and sensible heat), through flaws in measurements such as inability to capture low-frequency turbulent transfer, or (ii) accurately measured LE fluxes, and the missing energy can be explained otherwise (advection, storage, footprint mismatch)? If (i) is correct, then it is appropriate to take the relative proportion of latent to

Table 1 Tropical eddy covariance sites used for this analysis

| Site name	Biome type (all tropical lowland)	Latitude (°)	Longitude (°)	Reference
Africa				
Kissoko (KIS)	Humid eucalyptus plantation	−4.791389	11.982222	Unpublished
Americas				
Bananal Island (BAN)	Dry forest, seasonally flooded	−9.824417	−50.159111	Unpublished
Caxiuana (CAX)	Rainforest	−1.719720	−51.458890	Carswell *et al.* (2002)
Fazenda Nossa Senhora (FNS)	Pasture	−10.761806	−62.357222	von Randow *et al.* (2004)
Guyaflux (GUY)	Rainforest	5.277700	−52.928800	Bonal *et al.* (in press)
La Selva (LAS)	Rainforest	10.423333	−83.978889	Loescher *et al.* (2005)
Manaus C14 (M14)	Rainforest	−2.589200	−60.114900	Malhi *et al.* (2002)
Manaus KM34 (M34)	Rainforest	−2.609097	−60.209297	Araújo *et al.* (2002)
Reserva Jaru (RJA)	Seasonal forest	−10.083194	−61.930903	von Randow *et al.* (2004)
Reserva Pe-de-Gigante (RPG)	Savanna	−21.619472	−47.649889	da Rocha *et al.* (2004)
Santarem KM67 (S67)	Rainforest	−2.856667	−54.958889	Saleska *et al.* (2003)
Santarem KM77 (S77)	Pasture–agriculture	−3.011869	−54.536520	Sakai *et al.* (2004)
Santarem KM83 (S83)	Selectively logged rainforest	−3.018029	−54.971435	Goulden *et al.* (2004)
Oceania				
Cocoflux (COC)	Coconut forest plantation	−15.435000	167.185000	Roupsard *et al.* (2006)
South-East Asia				
Bukit Soeharto (BKS)	Regenerating rainforest	0.868889	117.052222	Huete *et al.* (2008)
Kog-Ma (KOG)	Monsoonal forest	18.800000	98.900000	Tanaka *et al.* (2003)
Lambir Hills (LAM)	Rainforest	4.200000	114.033333	Kumagai *et al.* (2005)
MaeKlong (MKL)	Deciduous forest	14.582500	98.850556	Huete *et al.* (2008)
Palangkaraya (PKA)	Peat swamp forest	−1.655000	114.036389	Hirano *et al.* (2007)
Sakaerat (SKR)	Dry forest	14.485000	101.925556	Huete *et al.* (2008)
Tak (TAK)	Monsoonal dry forest	16.622222	99.433333	Toda *et al.* (2002)
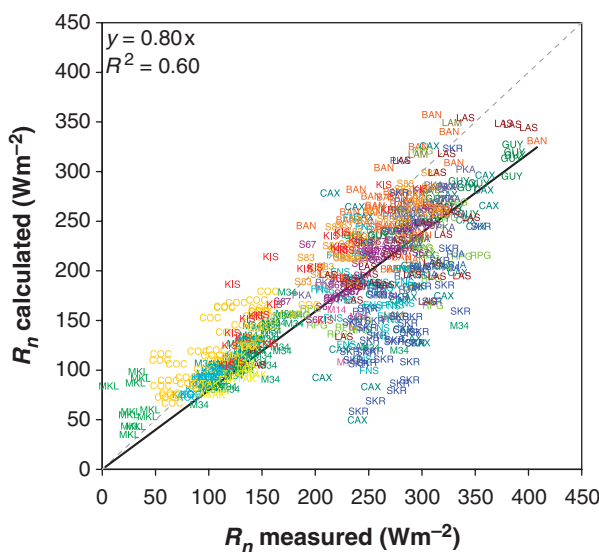
Fig. 2 Energy balance closure: measured R_n vs. calculated R_n (LE + H + G) for monthly averaged daytime values. The dashed line is the 1:1 line and the solid line is the linear regression forced through the origin.

sensible heat as the most robust field observation; if (ii) is correct, then the absolute measurement of LE is the most robust measurement. It is beyond the scope of this paper to discuss this issue in detail, but we suggest that (i) is more likely to be correct. Plausible physical mechanisms have been advanced for the transfer of turbulent energy at low frequencies (Finnigan *et al.*, 2003; Malhi *et al.*, 2004), whereas there is no convincing physical mechanism to explain consistent nonturbulent transfer of 20% of net radiative energy at the majority of flux sites. One consequence of adopting (i), however, is that model-based estimates of LE for any particular site will be approximately 25% higher than those derived from eddy covariance studies. Hence, to evaluate models against data, we focus on the partitioning of energy between sensible and latent heat fluxes, and therefore eliminate the issue of poor energy balance closure by using 'calculated' ($R_n = LE + H + G$) rather than measured R_n. Thus, our test of LE models is to evaluate how well they can detach LE from $LE + H + G$ based on environmental controls rather than assess why the eddy covariance method may inconsistently measure LE vs. R_n (for further discus-

sion, see Twine *et al.*, 2000). For all model tests vs. eddy covariance data, the models were run with calculated R_n.

Data: MODIS and ISLSCP-II

The normalized difference vegetation index (NDVI) and soil adjusted vegetation index (SAVI) (Huete, 1988; Los *et al.*, 2000) for the eddy covariance sites were determined from NASA's Moderate Resolution Imaging Spectroradiometer (MODIS). The Oak Ridge National Laboratory Distributed Active Archive Center (ORNL DAAC) subsets the full MODIS scenes (1200 km × 1200 km) to 7 km × 7 km areas containing the flux towers.

For production of the LE map for the Amazon, which we defined as Brazilian Legal Amazonia and the wet forest regions of Western Amazonia and the Guyanas (Soares-Filho *et al.*, 2006), we used 10-year input datasets for R_n, maximum T_a (T_{max}), and water vapor pressure (e_a) from the ISLSCP-II archive for 1986–1995 (Los *et al.*, 2000; Hall *et al.*, 2005). The ISLSCP-II data are $0.5°$ (~ 56 km) gridded monthly values. Surface Radiation Budget (SRB) data for R_n (Stackhouse *et al.*, 2000), which were based on meteorological inputs taken from Goddard Earth Observing System version 1 (GEOS-1) reanalysis datasets (Schubert *et al.*, 1993) by the Data Assimilation Office at NASA Goddard Space Flight Center, were subsampled from 1° to 0.5°. Cloud parameters and surface albedos were derived from the International Satellite Cloud Climatology Project (Pinker & Laszlo, 1992; Rossow *et al.*, 1996). ISLSCP-II T_{max} and e_a were from the Climate Research Unit Monthly Climate Data (New *et al.*, 2000). ISLSCP-II provided Fourier-adjusted, sensor and solar zenith angle corrected, interpolated, reconstructed (FASIR) adjusted NDVI. The enhanced vegetation index was not available (blue band) for this time period, but SAVI can be calculated instead (Huete, 1988; Los *et al.*, 2000). NDVI and SAVI were used for the flux sites as determined from MODIS as provided by the ORNL DAAC.

Models

Thirteen LE models were tested in this analysis (Table 2a and b). The models are described here in increasing complexity of parameterization (see Table 2a for abbreviations). Two LE models (HU, LR) were simple linear regressions based on T_a. HA and TH are based on T_a and day length. JH, PT, and TU are functions of R_n (or solar radiation) and T_a; PT includes a multiplier constant $\alpha = 1.26$ based on measurements of LE from a variety of well-watered vegetated and water surfaces. The FC model modifies the PT model with atmospheric moisture (VPD and RH) and vegetation indices (NDVI and SAVI). MB removes R_n, but includes VPD and r_c. PE

combines both energy and atmospheric vapor transport components (including u) to estimate potential LE. PM expanded on PE with aerodynamic resistance above the canopy (r_a) and canopy stomatal resistance (r_c). SW separated LE into soil evaporation (LE$_s$), which includes the aerodynamic resistance within substrate and canopy (r_w) and the surface resistance of the substrate (r_s), and canopy transpiration (LE$_c$), which includes the bulk boundary layer resistance of the vegetation (r_b) and r_c. Resistance terms were calculated following Shuttleworth & Wallace (1985) unless explicit resistance data were given; measured aerodynamic resistance showed good congruence with calculated aerodynamic resistance (data not shown). We used an artificial neural network (NN) trained to the entire dataset, computed in Tiberius (NeuSolutions), to represent a 'best possible' model that can reveal patterns and relative influences of the driving variables.

Analysis

We assessed LE at the tropical eddy covariance sites using three approaches: (1) evaluate the correlations between individual potential controls and LE; (2) train a NN model with all of the data for the output of relative importance; and (3) evaluate and compare errors and fits from a suite of LE models. A decoupling ω factor was calculated (see Table 2b) for each site to indicate the degree of influence (0 for fully coupled, 1 for fully decoupled) the shear-driven turbulent transfer over the canopy has over LE (Jarvis & McNaughton, 1986). The decoupling factor is another metric with which to compare the sites with one another. We first introduce the model performances at individual sites, and then present the results for all the sites combined. For combined-sites analysis, we randomly selected 12 months of data from each site to include so that sites with more data did not bias the results. We used all the data to evaluate the model performances. The models were judged in comparison by root mean squared error (RMSE), r^2, and slope for model-predicted LE vs. eddy covariance-measured LE. We forced the linear regression through the origin based on the logic of modeled LE expected to approach zero with measured LE. This zero-forcing results in the slope of the regression being a readily interpretable multiplying factor. The RMSE is the overall error in the prediction relative to the actual measured value. The r^2 assesses how well the model reflects the variation in the data, and the slope is a measure of overall accuracy. We based seasonality on PPT, but it should be noted that this may be an imprecise measure of soil moisture due to variability and uncertainty in soil water holding capacity, rooting depth, and water use efficiency.

Results

Correlations and NN ranks

R_n controlled LE regardless of the season across all sites combined. The evaporative fraction (LE/R_n) was 0.72, and R_n explained ($P < 0.05$) 87% of the variance (r^2) in monthly values across all sites (Fig. 3a). Although T_a explained most of the remaining variance ($r^2 = 0.13$;

$P < 0.05$), T_a also co-varied with R_n ($\rho_{X,Y} = 0.41$). R_n co-varied to a lesser extent with u ($\rho_{X,Y} = 0.26$), NDVI ($\rho_{X,Y} = 0.19$), VPD ($\rho_{X,Y} = 0.10$), and PPT ($\rho_{X,Y} = -0.07$). In a principal components analysis (Fig. 4), LE, R_n, T_a, NDVI, and u are situated closely along the first component axis (eigenvalue = 4.0), whereas VPD and PPT are relatively closer to the second component (eigenvalue = 1.2). LE was also correlated with NDVI

Table 2a Equations for the 13 latent heat of evaporation (LE) models analyzed

Thornthwaite (1948) – TH

$$1.067\Lambda\left(\frac{10T_a}{S_T}\right)^A$$

Penman-Monteith (1965) – PM

$$\frac{\Delta R_n + c_p\rho VPD/r_a}{\Delta + \gamma + \gamma(r_c/r_a)}$$

Penman (1948) – PE

$$\frac{\Delta R_n + 73.64VPD\rho\gamma(1 + 0.54u)}{\Delta + \gamma}$$

Priestley & Taylor (1972) – PT

$$\alpha\frac{\Delta}{\Delta + \gamma}R_n$$

Turc (1961) – TU

$$\frac{0.313T_a(R_s + 2.1)}{T_a + 15}$$

McNaughton & Black (1973) – MB

$$\frac{c_p\rho VPD}{\gamma r_c}$$

Hamon (1963) – HA

$$\frac{715.5\Lambda 0.61121\, e^{\frac{17.502T_a}{T_a+240.97}}}{T_a + 273.2}$$

Shuttleworth & Wallace (1985) – SW $PM_cC_c + PM_sC_s$

$$PM_c = \frac{\Delta R_n + (c_p\rho VPD - \Delta r_b R_{ns})/(r_a + r_b)}{\Delta + \gamma(1 + r_c/(r_a + r_b))}$$

Jensen & Haise (1963) – JH

$$0.41R_s(0.025T_a + 0.078)$$

$$PM_s = \frac{\Delta R_n + (c_p\rho VPD - \Delta r_w(R_n - R_{ns}))/(r_a + r_w)}{\Delta + \gamma(1 + r_s/(r_a + r_w))}$$

Hutyra et al. (2005) – HU

$$1.9 \times 30(0.3764T_a - 6.7084)$$

$$C_c = \left(\frac{1 + R_cR_a}{R_s(R_c + R_a)}\right)^{-1}$$
$$C_s = \left(\frac{1 + R_sR_a}{R_s(R_s + R_a)}\right)^{-1}$$

T_a linear regression (this study) – LR

$$8T_a - 80$$

$$R_a = (\Delta + \gamma)r_a$$
$$R_s = (\Delta + \gamma)r_w + \gamma r_s$$
$$R_c = (\Delta + \gamma)r_b + \gamma r_c$$

Neural network (this study) – NN

$(((((0.3 \times (((1.5NDVI-0.9) + (0.01R_n-4.1) + (-0.03T_a + 0.6) + (-0.2VPD + 0.3) + (-0.3u + 0.6) - 1.3) + 0.07)/2) + 0.5) \times 426.3) + 3.8$

Fisher et al. (2008) – FC

$$LE_s + LE_c + LE_i$$

$$LE_c = (1 - f_{wet})f_gf_Tf_M\alpha\frac{\Delta}{\Delta + \gamma}R_{nc}$$

$$LE_s = (f_{wet} + f_{SM}(1 - f_{wet}))\alpha\frac{\Delta}{\Delta + \gamma}(R_{ns} - G)$$

$$LE_i = f_{wet}\alpha\frac{\Delta}{\Delta + \gamma}R_{nc}$$

Table 2b Parameters and nomenclature for the latent heat of evaporation (LE) models

Parameter	Description	Value or equation
α	Priestley & Taylor (1972) constant	1.26
β	Units placeholder (or scaling coefficient) for f_{SM} (kPa)	1.0
γ	Psychrometric constant (kPa K^{-1})	0.066
ρ	Air density (kg m^{-3})	1.234
Δ	Slope of saturation-to-vapor pressure curve (kPa K^{-1})	$17.502 \times 240.97 \times es(T_a)/(T_a + 240.97)^2$
λ	Day length (fraction of day)	$f(R_s,$ latitude, day of year)
Ω	Decoupling factor (unitless)	$1/(1 + (\gamma/(\gamma + \Delta))(r_c/r_a))$
A	Fourth-order function of S_T	$f(S_T)$
c_p	Specific heat at constant pressure (J kg^{-1} K^{-1})	1005
f_c	Fractional total vegetation cover (unitless)	f_{IPAR}
f_{APAR}	Fraction of PAR absorbed by green vegetation cover	$1.4 \times SAVI - 0.05$
$f_{APARmax}$	Maximum f_{APAR} (unitless)	$\max(f_{APAR})$
f_g	Green canopy fraction (unitless, 0–1)	f_{APAR}/f_{IPAR}
f_{IPAR}	Fraction of PAR intercepted by f_c (unitless)	$1.0 \times NDVI - 0.05$
f_M	Plant moisture constraint (unitless, 0–1)	$f_{APAR}/f_{APARmax}$
f_{SM}	Soil moisture constraint (unitless, 0–1)	$RH^{VPD/\beta}$
f_T	Plant temperature constraint (unitless, 0–1)	$\exp(-((T_{max} - T_{opt})/T_{opt})^2)$
f_{wet}	Relative surface wetness (unitless, 0–1)	RH^4
G	Ground heat flux (W m^{-2})	Data
H	Canopy height (m)	Data
k_{PAR}	LAI coefficient	0.35
k_{Rn}	Light extinction coefficient (unitless)	0.6
LAI	Total (green + nongreen) leaf area index (m^2 m^{-2})	$-\ln(1 - f_c)/k_{PAR}$
NDVI	Normalized difference vegetation index (unitless)	$(NIR - R)/(NIR + R)$
NIR	Near-infrared wavelength or band (0.75–1.4 μm)	Data
r_a	Aerodynamic resistance above the canopy (s m^{-1})	$f(LAI, u, h, x)$
r_b	Bulk boundary layer resistance of the vegetation (s m^{-1})	$f(LAI, u, h, x,$ mean $r_b)$
r_c	Bulk stomatal resistance of the canopy (s m^{-1})	$f(LAI, u, h, x,$ mean $r_{stomata})$
r_s	Surface resistance of the substrate (s m^{-1})	$60.5 \times VPD - 16.5$ – fit to data
r_w	Aerodynamic resistance within substrate & canopy (s m^{-1})	$f(LAI, u, h, x)$
R	Red wavelength or band (0.63–0.74 μm)	Data
R_n	Net radiation (W m^{-2})	Data
R_{nc}	R_n to the canopy (W m^{-2})	$R_n - R_{ns}$
R_{ns}	R_n to the soil (W m^{-2})	$R_n \exp(-k_{Rn}LAI)$
R_s	Daily solar radiation (MJ m^{-2})	Data
RH	Relative humidity (unitless, 0–1)	Data
SAVI	Soil adjusted vegetation index	$(1.5)(NIR - R)/(NIR + R + 0.5)$
S_T	Thornthwaite heat sum	Data
T_a	Air temperature (°C)	Data
T_{max}	Maximum T_a (°C)	Data
T_{opt}	Optimum plant growth temperature (°C)	T_{max} at $\max(R_n T_{max} SAVI/VPD)$
u	Wind speed (m s^{-1})	Data
VPD	Vapor pressure deficit (kPa)	Data
x	Measurement height (m)	Data

($r^2 = 0.13$; $P < 0.05$). PPT and u were not correlated with LE, and this did not change across seasons.

Given that R_n was the dominant control on LE and co-varied with some of the other potential controls, we regressed the residuals of the linear relationship between LE and R_n (LE = $0.72R_n$) against the same controls to determine if we could explain any additional variance (Fig. 3b). There was no correlation with T_a regardless of the season. VPD explained some of the variation ($r^2 = 0.14$; $P < 0.05$) in the residuals, followed by NDVI ($r^2 = 0.09$; $P < 0.05$), PPT ($r^2 = 0.06$; $P < 0.05$), and u ($r^2 = 0.04$; $P < 0.05$), especially in the dry season.

The degree to which these controls interact with the vegetation is dependent on how coupled, or decoupled, the vegetation is to the surrounding atmosphere. Wetter sites were more decoupled ($P < 0.05$) with generally open stomata and were subsequently controlled largely by R_n (Fig. 5). Similarly, as u increases, so too does the
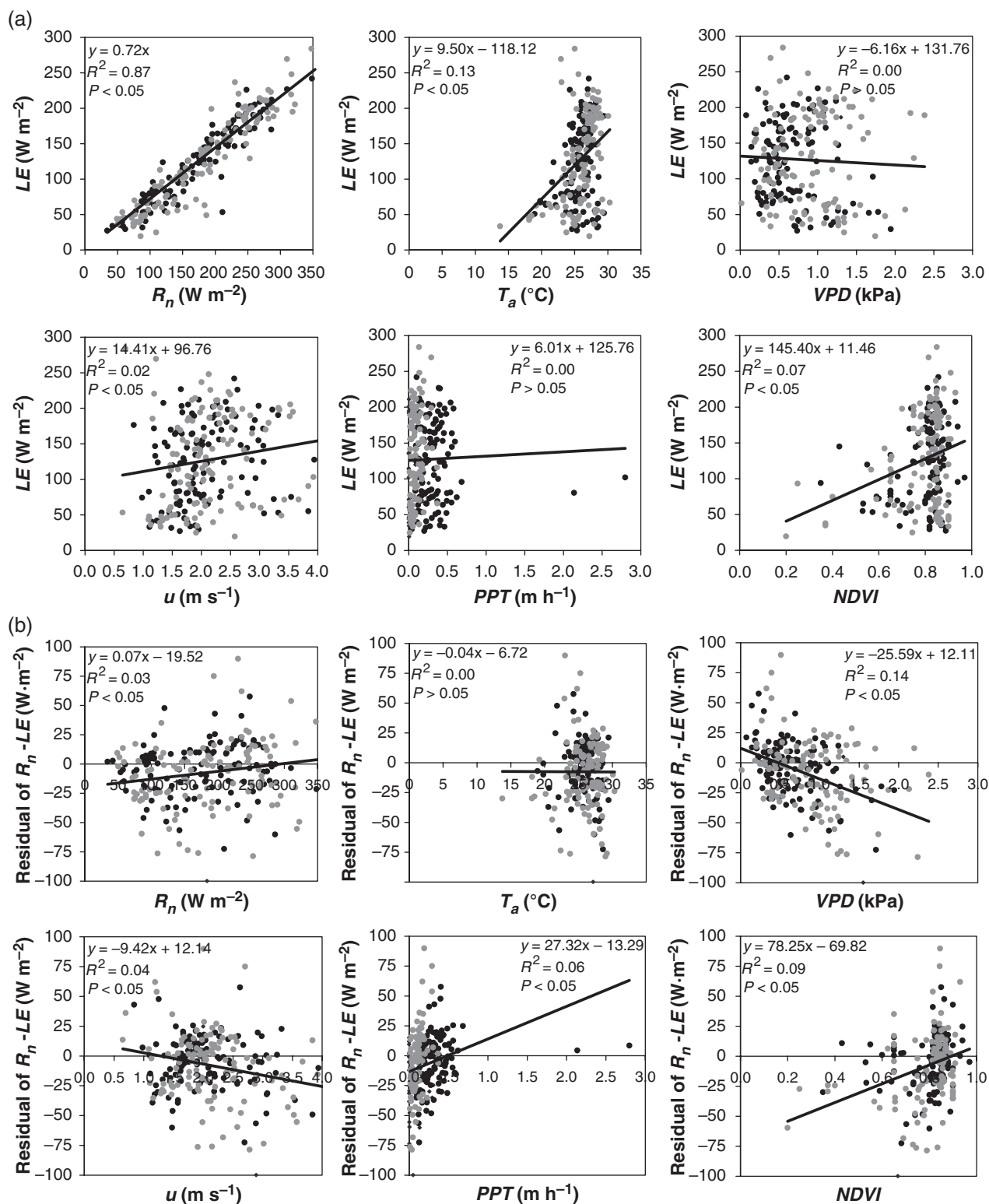
(a)

(b)

Fig. 3 (a) Latent heat of evaporation (LE) vs. R_n, T_a, vapor pressure deficit (VPD), u, precipitation (PPT), and normalized difference vegetation index (NDVI) for all 21 tropical eddy covariance sites (12 data months chosen at random from each site). (b) Residuals of R_n as a function of LE ($R_n = 1.34LE$) minus R_n vs. R_n, T_a, VPD, u, PPT, and NDVI. Symbols are for dry (gray) and wet (black) seasons.
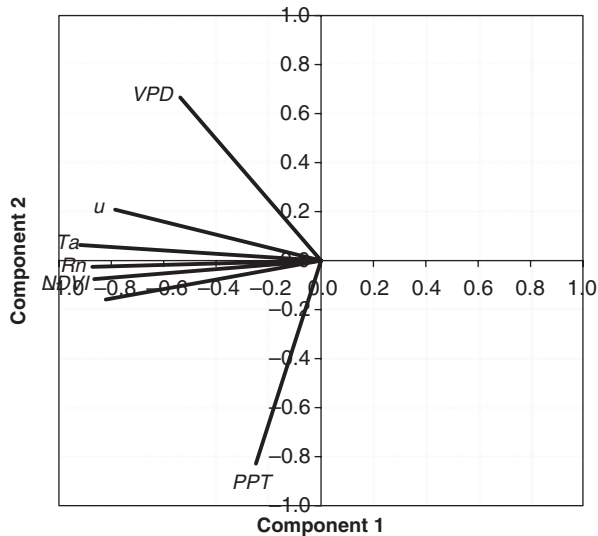
Fig. 4 Principal components analysis shows latent heat of evaporation (LE), normalized difference vegetation index (NDVI), R_n, T_a, and u near to the first component axis, while vapor pressure deficit (VPD) and precipitation (PPT) are relatively nearer to the second component axis.
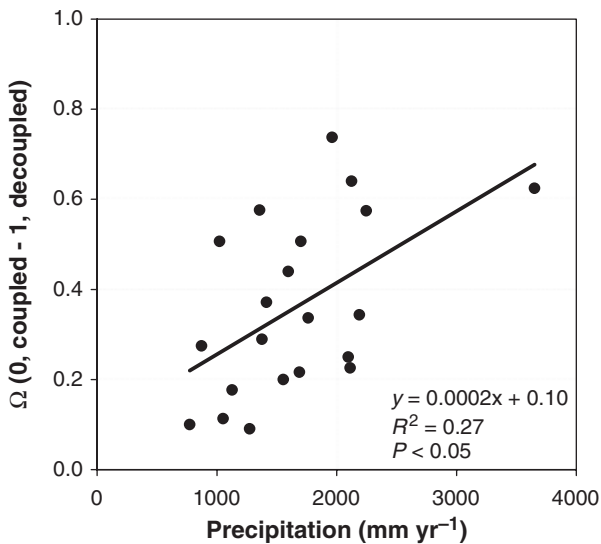

Fig. 5 The decoupling coefficient (Ω) increases at wetter sites (site average).

mixing between the land and atmosphere, thus increasing the degree of coupling between the two ($\Omega = -0.2u + 0.7$; $r^2 = 0.18$; $P < 0.05$). The decoupling coefficient is dependent on r_c, and we were able to invert the Penman–Monteith equation (1965) to estimate r_c, given the extensive dataset of LE measurements. We compared the inverted Penman–Monteith r_c with the same environmental variables and found that the strongest correlation was with VPD ($r^2 = 0.21$; $P < 0.05$; $r_c = 237.1 \times \text{VPD} + 1.2$).

The NN searched for the combination of weights assigned to any number of dependent variables (neurons) to minimize the error in predicting the independent LE measurements. The learning rate determined the magnitude of the change. In addition to the final NN equation (Table 2a), one of the final outputs was a ranking of the importance for any combination of each of the input variables. The top ranked primary input was R_n followed by VPD, NDVI, and u. PPT and T_a were ranked of negligible importance.

LE models – individual sites

Site data ranged from sparse measurements for less than a year to continuous measurements over multiple years (Fig. 6); the FC model is included for comparison of the data with a model. The sites are organized approximately from wettest to driest (although RJA, a dry site, is grouped with the wet sites due to an inflated evaporative fraction from limited data). The best performing models – NN, FC, TU, PT, and JH – were consistent across most sites, whereas the T_a-based models and the resistance models showed variable performance across the sites (Fig. 7). The R_n-based models generally had the lowest RMSEs and highest r^2s, but not necessarily the best slopes. The sites in Fig. 7 are arranged from left to right in descending order of evaporative fraction, which is how much R_n is used for LE and a general indication of site wetness and seasonality. Particularly for the R_n-based models, the RMSE tended to increase and the slope and r^2 decrease moving from wet to seasonal sites – this trend can be seen in Fig. 7 in the upward rise from left to right for RMSE and vice versa for r^2 and slope within each model. We examine each site in more detail below, moving in descending order of evaporative fraction.

La Selva (LAS) (rainforest). LAS had the most variation in LE (standard deviation = 81 W m^{-2}), the highest LE overall (and subsequently the highest absolute RMSEs for many of the models, but not as a percentage of average), and was nearly always at potential LE as was evident in the performance of the R_n-based models. Still, PT, JH, PE, and PM had their lowest RMSEs at LAS, but NN and TU had their highest RMSEs at this site. The T_a-based models followed the variation in LE, but when LE increased dramatically, T_a increased only mildly resulting in poor RMSEs and slopes.

Reserva Jaru (RJA) (seasonal forest). Variance in LE was small (16.9 W m^{-2}), even with sparse data. Ω was relatively high (0.65), indicating less dependence on shear-driven turbulence, especially as RJA is a dry site and uses much of the R_n on LE. NN, PE, and LR had

their lowest RMSEs, and PE had its best slope, but PM and SW had their worst slopes at RJA.

Santarem KM83 (S83) (selectively logged rainforest). This was the best site for the FC model for RMSE and slope. S83 was selectively logged in September 2001 (Goulden *et al.*, 2004). Three months after the logging, there was a drop in LE that the FC model failed to match; model accuracy resumed when LE increased the following month. All of the models performed better than average at S83.
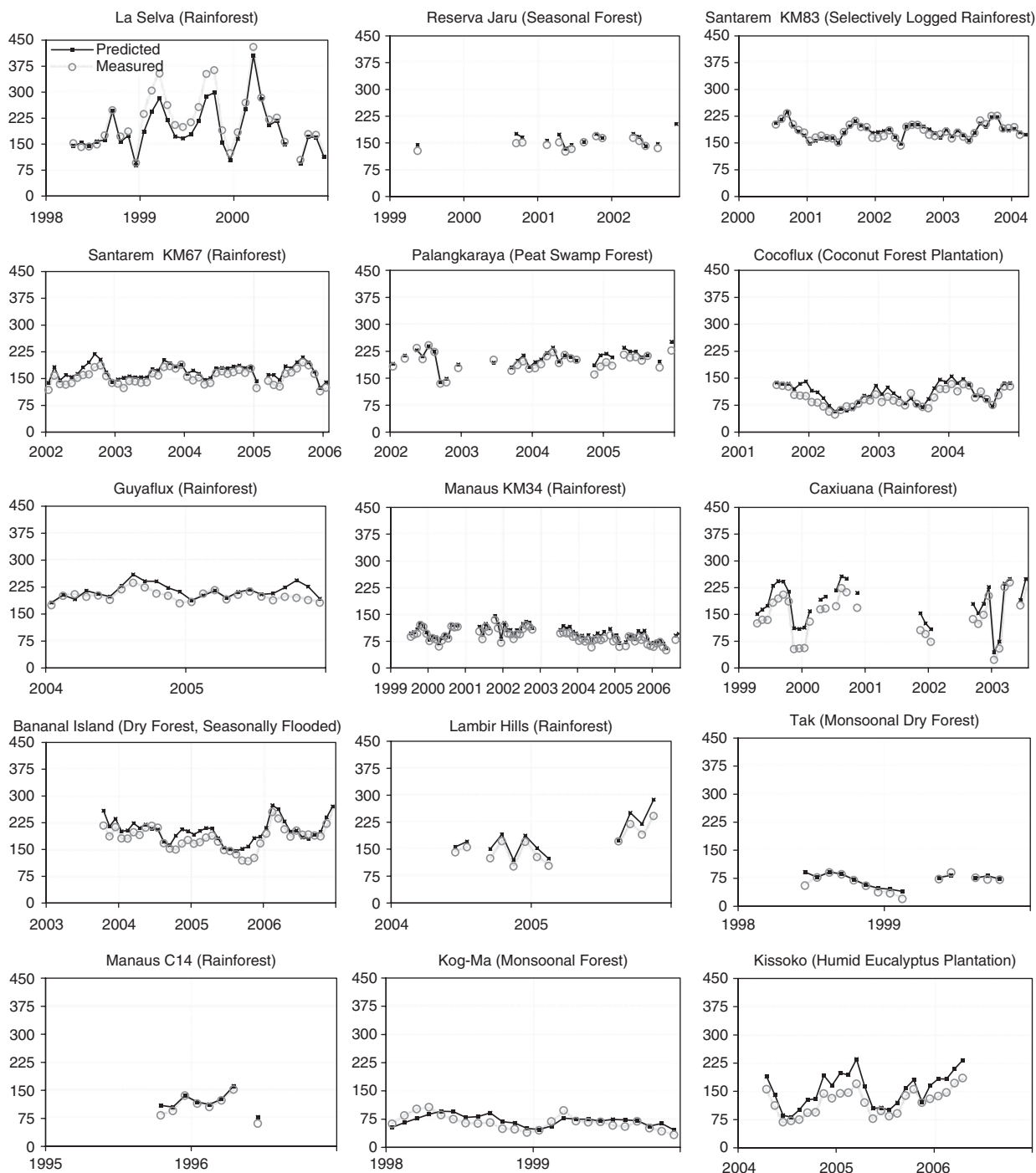

Fig. 6 Time series of tower measurements and model predictions at each site sorted in descending order by evaporative fraction. The *y*-axis is latent heat of evaporation (LE) (W m^{-2}) and *x*-axis is year. Open circles are observed and closed squares are predicted LE based on the FC model.
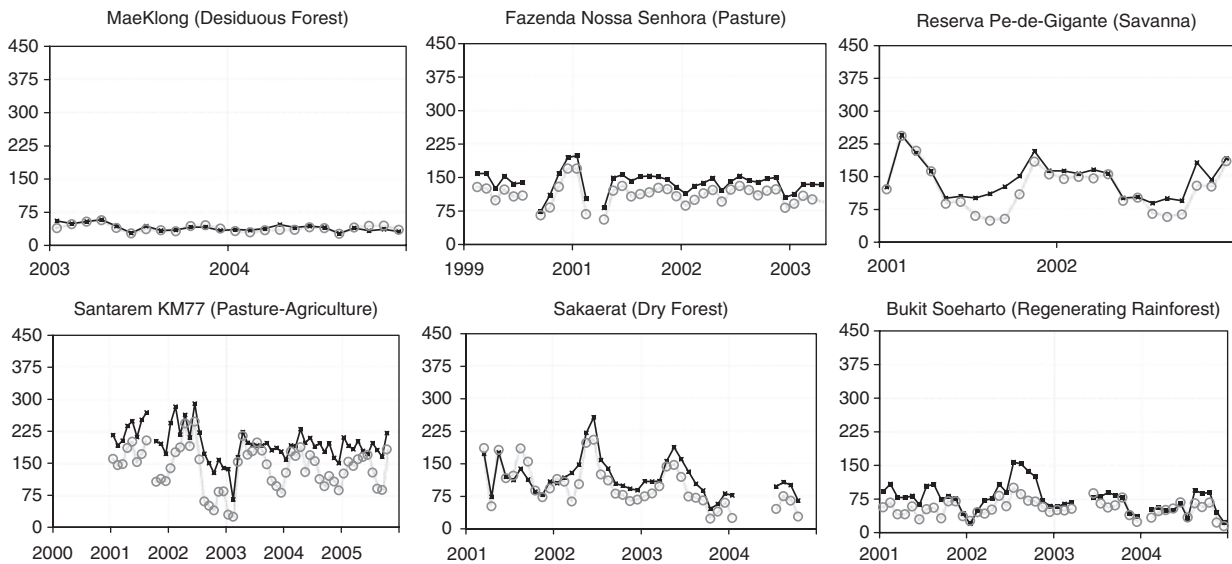
Fig. 6 Continued.

Santarem KM67 (S67) (rainforest). The T_a-based models performed best at S67 for RMSE, r^2, and slope, indicating that T_a had relatively high control of LE. This was particularly the case for the HU model, which was developed at S67. All of the models performed better than average at S67.

Palangkaraya (PKA) (peat swamp forest). The T_a-based models performed worst at PKA, because LE was relatively insensitive to T_a at this site. The resistance-based models also performed particularly poorly at PKA. The R_n-based models performed well here.

Cocoflux (COC) (coconut forest plantation). Although COC was the only Oceania site, the pattern of LE at COC was similar to that at S67 in the Amazon – consistently, but mildly seasonal; both sites had the same Ω (0.34), which was the median value for the entire dataset. The resistance-based models were particularly sensitive to changes in r_c at COC because of the relatively uniform canopy (low species diversity) and high sensitivity of stomata to VPD. Subsequently, this was the best site for the MB model for RMSE and for the PM model for slope. The T_a-based models predicted an inverse of the observed LE (i.e., high prediction when low observed, low prediction when high observed).

Guyaflux (GUY) (rainforest). GUY was among the sites with least variation in LE (standard deviation = 17 W m^{-2}). A slight deviation or over-sensitivity to one of the meteorological variables could lead to poor model performance statistics, which occurred when one

data point caused a significant drop in r^2 for many of the models. This point was a short period where it was particularly hot and dry, but LE did not increase; H at this point was the third highest in the entire dataset. GUY was the worst site for r^2 for nearly all of the models.

Manaus KM34 (M34) (rainforest). This site contributed the most data from generally continuous long-term measurements (1999–2007). M34 is often used as the benchmark average estimate of LE for the Amazon at 100 W m^{-2}. The average LE at M34 was 98 W m^{-2} from 1999 to 2003, but dropped to 72 W m^{-2} during 2003–2007; the overall average was 86 W m^{-2}. All of the models had relatively higher RMSEs here, but higher r^2s as well. M34 had the third highest Ω (0.62), and the resistance-based models had their worst slopes at M34. The T_a-based models performed relatively well at M34.

Caxiuana (CAX) (rainforest). Although the variation in LE was the second highest (standard deviation = 63 W m^{-2}), CAX had very strong wet seasons and weak dry seasons, and hence it tended to be near potential LE. This was the best site for r^2 for the NN and FC models and among the worst sites for the T_a-based models.

Bananal Island (BAN) (dry forest, seasonally flooded). All of the models had some difficulty matching the variation in LE here, especially the decline in LE in the late dry season. The R_n- and T_a-based models had relatively low RMSEs, but poor r^2s. The best slope for MB but worst
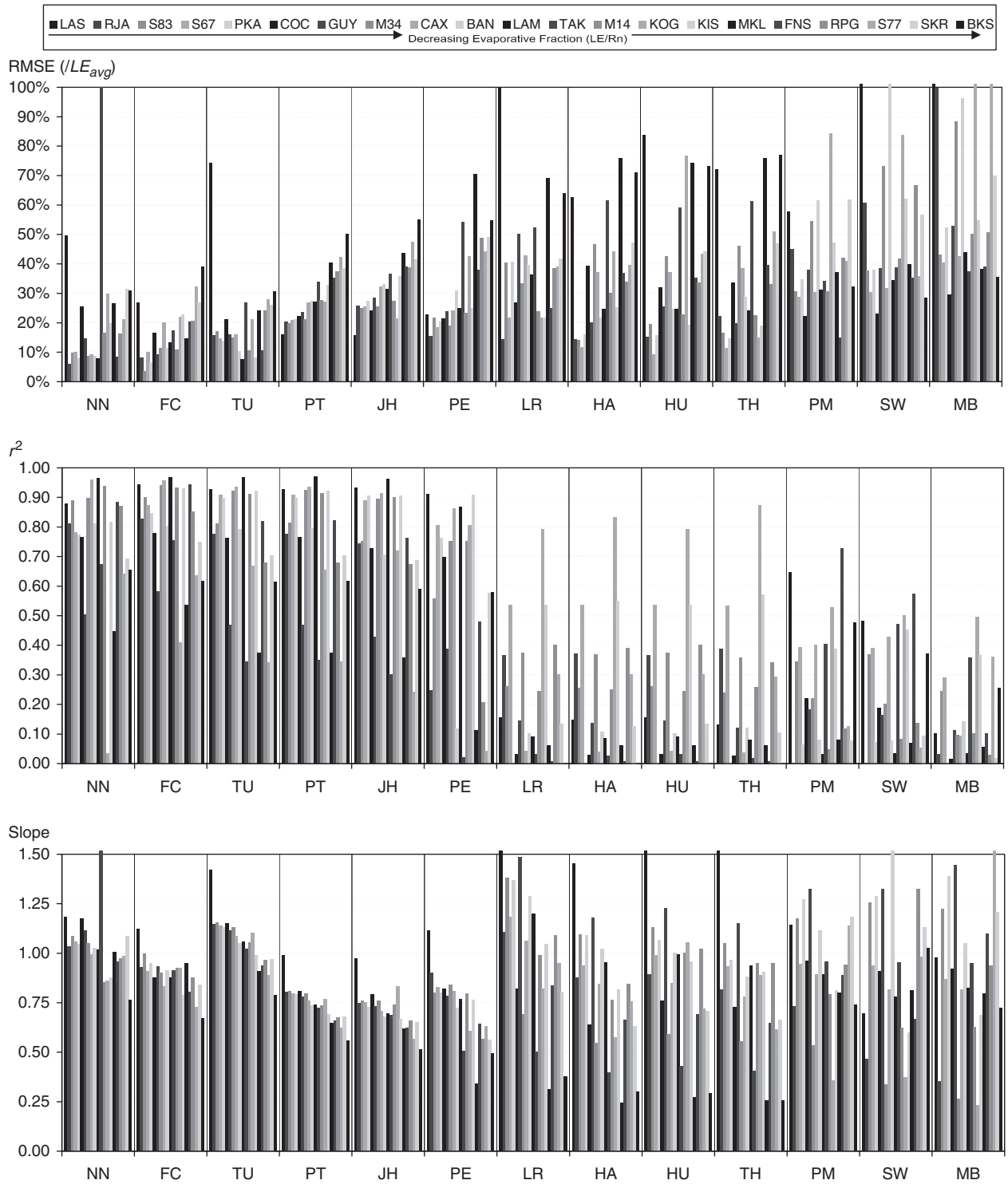
Fig. 7 Root mean squared error (RMSE) [as a percentage of average latent heat of evaporation (LE) for each site], correlation coefficients (r^2), and slopes for each of the models at each of the 21 tropical eddy covariance sites sorted in descending order by evaporative fraction. Abbreviations for the sites and models can be found in Tables 1 and 2, respectively.
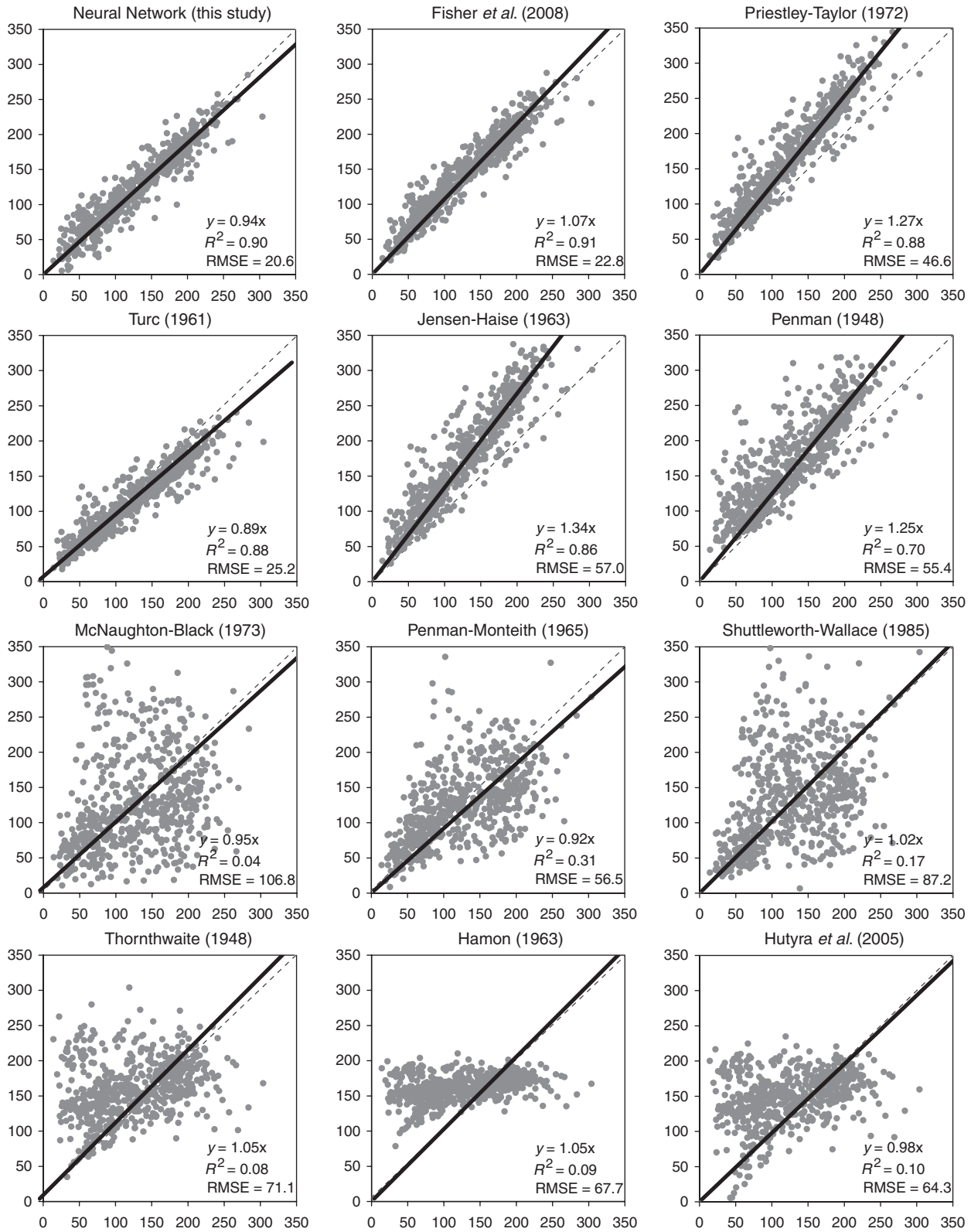
Fig. 8 Measured latent heat of evaporation (LE) (*x*-axis) vs. predicted LE (*y*-axis) for 12 LE models (the empirical linear regression from T_a based on this study can be seen in Fig. 3) at 21 tropical eddy covariance sites. The dashed line is the 1 : 1 line and the solid line is the linear regression forced through the origin.
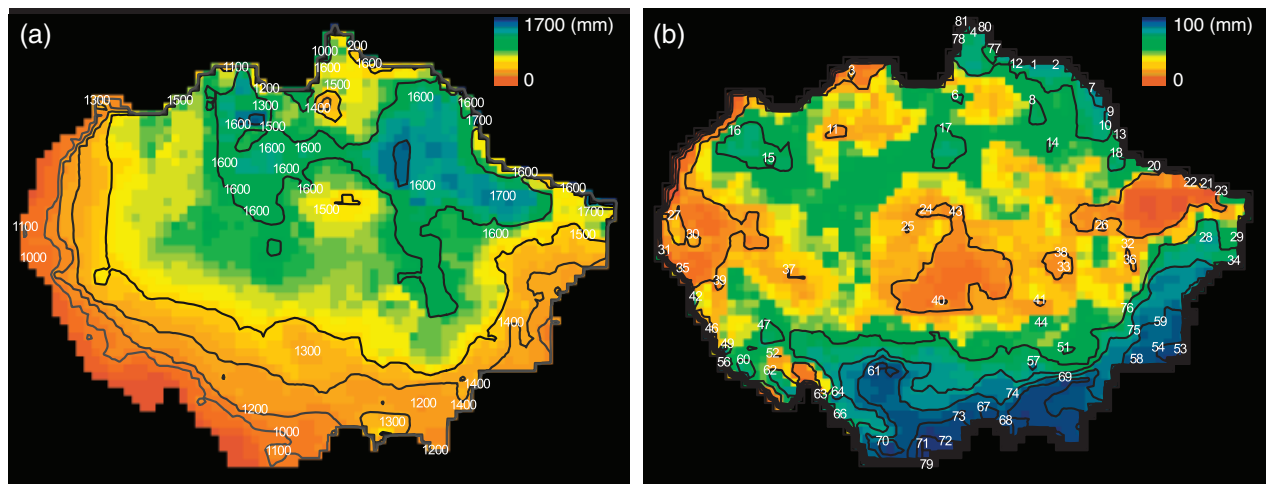
Fig. 9 (a) 10-year (1986–1995) mean annual latent heat of evaporation (LE) for the Amazon Basin based on the FC model with ISLSCP-II data. Contour lines follow 100 mm intervals. (b) 10-year (1986–1995) mean annual amplitude in LE for the Amazon Basin.

slope for SW was at BAN. The T_a-based models had relatively good slopes here.

Lambir Hills (LAM) (rainforest). The R_n-based models had their highest r^2s at LAM, and lowest RMSE for the TU model. The slopes were generally good for the T_a-based models.

Tak (TAK) (monsoonal dry forest). TAK had the third lowest Ω (0.11), and the resistance-based models had their best slopes at TAK (conversely compared with M34); this was the best site for slope for PM. Further, the r^2s were good for the resistance-based models, but among the worst for R_n- and T_a-based models. The NN model performed unusually poor here with its worst RMSE and slope at TAK.

Manaus C14 (M14) (rainforest). M14 had the fourth highest Ω (0.58) behind M34. Similarly, the R_n- and T_a-based models had relatively high r^2s, the resistance-based models performed poorly. All of the models tended to have lower RMSEs than average at M14.

Kog-Ma (KOG) (monsoonal forest). LE at KOG was particularly sensitive to T_a. This was the best site for r^2 for the T_a-based models and for MB, but the worst for NN and FC. The resistance-based models had poor RMSEs at KOG, and this was the site of worst RMSE and slope for the PM model.

Kissoko (KIS) (humid eucalyptus plantation). KIS was the only Africa site, but the data were comparable with the mean of the entire dataset for most variables. KIS

experienced humid advection that caused the FC model to over-predict LE at times. The T_a-based models performed relatively well here. The TU model performed particularly well at KIS with its best RMSE and slope.

MaeKlong (MKL) (deciduous forest). MKL had the lowest variance in LE of the entire dataset (standard deviation = 8 W m^{-2}) and second lowest Ω (0.10). All but the resistance-based models had worse RMSEs at MKL than average, especially for PE and HA. The T_a-based models had their worst slopes at MKL, but the NN model had its best slope here. The r^2s for all the models were lower than average.

Fazenda Nossa Senhora (FNS) (pasture). Although FNS was a pasture site, the variance in LE was the median of the entire dataset (standard deviation = 24 W m^{-2}), and it had the highest Ω (0.74). The PM model performed particularly well at FNS with its best RMSE and r^2 here; the SW model also had its best r^2 at FNS due largely to the relatively high influence of soil evaporation for the sparse canopy.

Reserva Pe-de-Gigante (RPG) (savanna). As a savanna near the Tropic of Capricorn, RPG was the furthest site from the equator in this analysis. RPG had a low Ω (0.18) and high variance in LE (standard deviation = 53 W m^{-2}). The R_n-based models had problems with the seasonal drought because actual LE was much less than potential LE in the dry season. The T_a-based models had relatively high r^2s, however.
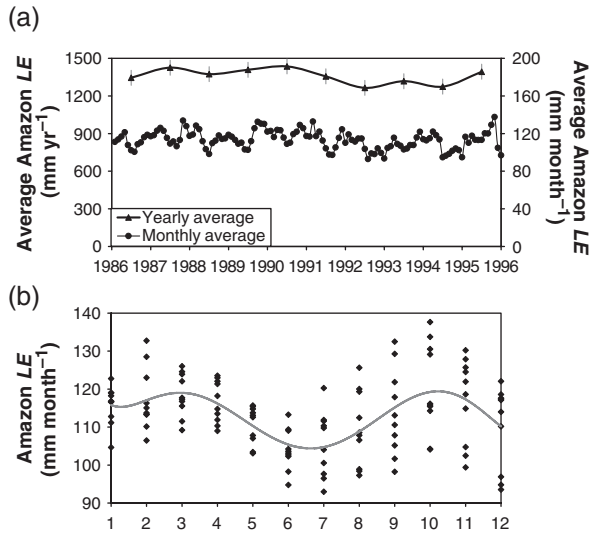
(a)

(b)

Fig. 10 (a) 10-year (1986–1995) mean annual and monthly latent heat of evaporation (LE) for the Amazon Basin; *X*-axis is year. (b) Monthly pattern of LE with yearly variation for the Amazon Basin; *X*-axis is month. ISLSCP-II data drive the FC model for these results.

Santarem KM77 (S77) (pasture–agriculture). S77 was the site of worst r^2 for the R_n-based models, and the worst RMSE and slope for the MB model. There was extensive disturbance at the site during the measurement period, and it was difficult to separate error in model predictions from disturbance vs. natural variance.

Sakaerat (SKR) (dry forest). SKR was similar in location to MKL and had lowest Ω (0.09), but had one of the highest variances in LE (standard deviation = 50 W m^{-2}). All the models performed worse than average at SKR for RMSE, r^2, and slope.

Bukit Soeharto (BKS) (regenerating rainforest). The resistance-based models had better than average RMSEs and BKS, and the SW model had its best slope here. All the other models, however, had their worst RMSEs and slopes at BKS.

LE models – all sites/data

The best performing models were the NN, FC, and TU models. The NN model should perform best overall (smallest RMSE, highest r^2, slope closest to 1) because it was empirically fitted to the data, and the only model tested here that was empirically fitted to the data – this is useful for comparison with the more mechanistic models. NN had the lowest RMSE (20.6), among the best slopes (1.04), and highest r^2 (0.90; the r^2 for the FC

model was 0.91, but this is not statistically significantly greater than the r^2 for NN).

The three models that relied on radiation and T_a alone were PT, TU, and JH. The r^2s were similar (0.88, 0.88, 0.86, respectively), but the RMSE and slope were better for TU (25.2 and 1.10). The JH model performed the poorest of the three. The r^2 increased slightly in the wet season for all three models. PE, which relied additionally on VPD and u, had a slope and RMSE that were similar to those for PT, but the r^2 (0.70) was significantly lower. The equation for PT in Fig. 8 is presented as $y = 1.27x$, where y is the predicted LE and x is the measured LE. This slope or multiplier value is similar to the value of the PT α coefficient (1.26). Therefore, for these data, the PT multiplier of 1.26 is unnecessary (or should be equal to 1) and actually leads to over-prediction by ~ 1.26.

The three models that relied on one or more resistance terms are MB, PM, and SW. All three models had higher values of r^2 (i.e., improved goodness of fit) in the dry season. The best performing resistance-based model was PM, which had a relatively low RMSE (56.5) and good slope (0.92), but the r^2 was relatively poor (0.31). The SW model performed slightly worse, and the MB model, which does not include R_n and is therefore heavily dependent on VPD, performed the poorest of all of the models.

The T_a-based models (LR, TH, HA, and HU) reflected very little of the variation in LE for the combined sites analysis ($r^2 = 0.08$–0.10), though this improved slightly in the dry season. Generally, T_a does not vary much in the tropics (20–30 °C, daytime average), whereas LE varies extensively. The T_a models accurately predicted mean LE over the entire time period of measurements, however, and the slopes were generally good (0.78–0.84) and the RMSEs were relatively low (64.3–71.1).

Amazon map

We generated an Amazon LE map product from the FC model, which was among the best models overall for predicted LE vs. measured LE. The FC model was selected against the NN model, because the NN model resulted in unrealistic values, especially outside of the Amazon due to its empiricism to the individual sites (data not shown). The FC model may be scalable beyond the eddy flux footprint, because it is driven primarily by large-scale parameters, such as radiation, temperature, and humidity. The FC model was driven with data from the ISLSCP-II archive and remote sensing data, which were available across the Amazon; therefore, we were able to create a map of LE across the whole Amazon Basin, based on the FC model to explore the regional variations of this flux.
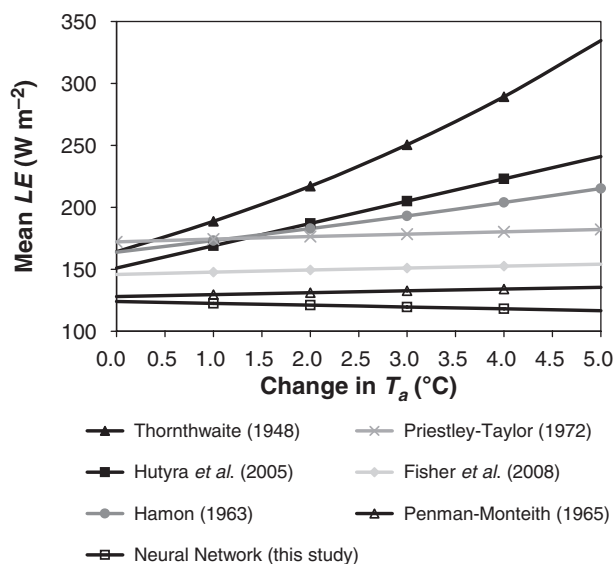
Fig. 11 Mean latent heat of evaporation (LE) for seven LE models across 21 tropical eddy covariance sites with changing T_a.

First, we compared the pixel-modeled LE values with the tower measurements, though this comparison is not conclusive due to a large number of sources of error: (A) the pixel size covered a larger area than the eddy flux tower footprints; (B) the temporal mismatch between the ISLSCP-II dataset (1986–1995) and FLUXNET dataset (1995–2007) – we used the average monthly values for the entire 10 years of ISLSCP-II and compared them with the average monthly values for the entire flux dataset at each site, but any major temporal changes in the sites (e.g., warming, drying, annual/decadal events) would lead to large mismatches; (C) uncertainty in the ISLSCP-II data – i.e., 10–15 $W\,m^{-2}$ for radiation (Stackhouse et al., 2000); (D) uncertainty in the FLUX-NET data; and (E) uncertainty in the FC model (see Fig. 8). The measured LE at the eddy covariance sites tended to be less than the pixel-estimated LE, although both the site-calculated R_n and measured R_n were larger than the pixel R_n (site-calculated $R_n = 1.23 \times$ pixel R_n; site-measured $R_n = 1.59 \times$ pixel R_n) – due to the large variance in these data comparisons, these relationships were not statistically significant. FC-predicted LE was 89% of R_n for the ISLSCP-II data (FC-predicted LE at the sites was 81% of calculated R_n).

Over the 10-year span (1986–1995), Amazon LE was relatively spatially homogeneous at the pixel size of $0.5°$ throughout the basin (Fig. 9a). The mean LE for this spatial-temporal period was 1370 $mm\,yr^{-1}$, median was 1437 $mm\,yr^{-1}$, standard deviation was 183 $mm\,yr^{-1}$, and mode was 1478 $mm\,yr^{-1}$ (107 pixels). The seasonal amplitude showed no pattern, east–west or otherwise for the entire 10 years other than in the south and southeast where the Amazon delineation (the boundary

of the Amazon as defined by Soares-Filho et al., 2006) included some pasture and savanna. The spatial patterns and distributions of LE were driven primarily by similar spatial patterns and distributions in solar radiation. Although there were distinct spatial patterns in mean values of LE, there were no clear patterns in seasonal amplitude except at the dry margins in the south and east (Fig. 9b). The highest mean values of LE are in the north and northeast. These are regions that have high radiation input in the dry season (July–November), when the lack of clouds combines with relatively high sun angles (near-equatorial location), while at the same time, there is little evidence of dry season restriction of water supply (e.g., CAX, GUY, S67, S83). The southern Amazon also has a sunny dry season (May–September), but this period coincides with relatively low sun angle and shorter days (sun is overhead near the Tropic of Cancer), leading to little increase in solar radiation in the dry season. Seasonal variability in NDVI increases in importance at the dry forest–savanna transition at the south-east margins, where intensity of water deficit drives a strong annual cycle in vegetation phenology.

There is slight interannual variability in LE totals (Fig. 10a). These are driven by radiation input, with an implicit assumption being that any interannual variability in water stress would be reflected in either VPD or NDVI data. In the period 1991–1994, there was a decline in LE for 4 years due likely to global dimming from the Mt Pinatubo eruption in 1991 (Fisher et al., 2008), returning to previous averages in 1995. Monthly minima in this 4-year low were not significantly less than other monthly minima from previous years; the maxima were somewhat reduced, however, suggesting a reduction in dry season radiation input. Our modeled interpolation of Amazon LE followed a seasonal cycle (Fig. 10b): basin-wide LE is lowest in May–September, when the sun is overhead close to the Tropic of Cancer (the bulk of Amazonia lies south of the equator).

Discussion

Controls on LE

It is known that R_n controls LE in most of the wet tropics, but the degree to which and the temporal consistency vary in the literature (Hasler & Avissar, 2007). For the sites and temporal period analyzed here, LE used 72% of R_n with seasonal consistency. R_n was the primary driver and the canopy was mainly decoupled from the atmosphere, especially at wetter sites. VPD was the most important control in the

residual analysis, which is consistent with field observations throughout the Amazon (Granier *et al.*, 1996; Williams *et al.*, 1998; Malhi *et al.*, 2002). NDVI was also important in the residual analysis, but the strength of that regression for both VPD and NDVI decreased if the driest sites are removed from the analysis (and the r^2 for R_n increases to 0.90).

T_a explained most of the remaining variance in LE after R_n, yet was negligible in both the residual analysis and the NN ranks. Furthermore, the T_a-based models provided little predictive power at most sites. The residual analysis, NN and model analysis contradict the initial regression analysis with regards to T_a. It may be more likely that T_a is controlled by R_n, but has minimal control over LE. The average Bowen ratio (H/LE) is 0.3, so an increase in R_n leads to a much larger absolute increase in LE than in H (and hence T_a). Hutyra *et al.* (2005) reported a T_a-based model with a tropical frame of reference that outperformed the other T_a-based models, particularly at their S67 site. We found that the T_a-based models tended to improve with decreasing site wetness.

We expected LE to change in response to PPT, though it has been found that tropical forests can continue LE during dry periods from residual soil moisture and deep-water access (Nepstad *et al.*, 1994; Saleska *et al.*, 2007). Across all sites, we found no positive correlation between LE and PPT, and found that LE continued in the dry season sometimes at an even higher rate than during the wet season. We tested for a temporal lag between LE and PPT due to differences in time scales but found no improvement in correlation. At extremely wet sites, a drop in PPT did not necessarily lead to a drop in LE because the lower PPT was still very high. At the driest site (RPG – savanna), LE and PPT were correlated ($r^2 = 0.28$; $P < 0.05$); r^2 was 0.18 for RJA, but there was no correlation at BAN or FNS. In the residual analysis, PPT was minimal ($r^2 = 0.06$), but was more correlated in the dry season ($r^2 = 0.26$).

An important caveat with the results of the aggregated site data is that the sites are not necessarily representative samples of the tropics as a whole. The majority of the sites were within Amazonia, and those sites were generally located centrally or to the east. A simple comparison between the sites map in Fig. 1 with the mean annual LE map in Fig. 10a shows that the sites were generally in regions of relatively high LE. We can compare the site locations with other gridded maps of T_a, PPT, NDVI, VPD, and u, but these comparisons reinforce the initial caveat. Also, we assumed uniform data quality, but this is not necessarily the case. Unfortunately, it was very difficult to design appropriate weights relative to the data quality for each site. Although we were able to account for much of the

variability in LE, it may not be possible to account for 100% because of the intrinsic noise associated with turbulence sampling variability for eddy covariance measurements (Wilson *et al.*, 2002).

Models

Why do some models perform better than others? First, all models are built for a purpose and all models have pros and cons. The T_a-based models, for instance, were built without R_n not because R_n is unimportant, but because these data are not always available, whereas T_a is much more readily available (Hutyra *et al.*, 2005). Conversely, the resistance-based models were built to be more theoretically accurate, though in so doing more difficult to parameterize (e.g., Farahani & Ahuja, 1996; Alves & Cameira, 2002). Because radiation was the dominant control for these sites, the resistances added little to the explanatory power, instead providing noise that accompanied the propagating error of additional parameters (Fisher *et al.*, 2005).

The radiation-based models all performed well, but the JH model was not quite as good as the others because of its structure. The PT model, for example, has fewer empirical constants and is therefore less constrained to the sites where the empirical constants were formulated; it performed best relative to the number of inputs required. Adjustment of the α coefficient closer to 1 would provide a better fit, but knowledge *a priori* of how to scale the PT model is lacking. Many researchers have scaled down the α coefficient based on soil moisture (Fisher *et al.*, 2005). The PT equation estimates potential LE assuming well-watered soil; therefore; downscaling PT should be dependent on downscaling potential to actual LE. In the tropical sites of this analysis, however, soil moisture (or lack thereof) is unlikely to lead to reduction in the α coefficient by 80% (from 1.26 to 1) because these sites are generally wet. However, the 80% PT result may be related to the energy balance closure – calculated R_n was on average 80% of measured R_n (Fig. 2).

The FC model modifies the PT model based on atmospheric moisture and canopy ecophysiology – these constraints provide the mechanistic basis upon which to scale the PT model. If the constraint functions are instead used to modify a different base LE model, then that model would improve as well. The NN model was the best model overall, but it was entirely empirically fit to the data with no mechanistic representations. When the model is applied to sites outside the tropics, then the performance is much weaker (data not shown). Still, it is encouraging for model development that the empiri-

cal NN model performed only marginally better than the FC model.

The FC model substitutes canopy conductance and soil moisture – arguably the two most difficult-to-characterize parameters (Raupach & Finnigan, 1988) – with its constraint functions. Canopy conductance is generally calculated as a scaling function from stomatal conductance (Shuttleworth & Wallace, 1985). Scaling stomata to canopy may be relatively straightforward for monoculture agricultural systems or dominant successional type ecosystems. In the tropics, however, scaling stomata to canopy is more challenging because of high species diversity and complex canopy structure. Hence, the resistance-based models performed poorly in this analysis. Still, LE from the radiation-based models can be used to invert the PM model to calculate and average r_c. The inverted PM r_c was correlated with the LE_i component of the FC model ($r^2 = 0.41$; $P < 0.05$).

Modeling soil moisture is error-prone for three reasons. First, the vertical and horizontal profiles of soil moisture are highly sensitive to model parameterizations (e.g., Richard's equation) and difficult to validate with field data (Robock et al., 1995). Second, root depth profile modeling is not well established (Grant, 1998). Finally, even if soil moisture and root profiles were well characterized, how the plants actually use soil moisture varies from species to species depending on the life strategy and water use efficiency (Goulden, 1996; Kang et al., 2002). The implicit assumption within the FC model is that significant changes in water supply would manifest themselves as detectable changes in atmospheric moisture and NDVI; the FC model does not explicitly model soil moisture status.

With changing global climate, how will tropical LE change, especially with warming temperatures? How do the LE models respond to perturbations in temperature and other variables? Certainly, it is difficult to predict the dynamic changes, resiliency, and adaptation of ecosystems to climate change – one cannot simply increase T_a in the models while holding all other variables as constants and expect realism. Still, it is possible to test the sensitivity of the LE models to changes in T_a. The average daytime monthly T_a across all sites in this analysis was 26 °C. We increased monthly T_a by 5 °C at 1 °C increments and observed the response in overall mean LE by the three T_a-based models (TH, HU, HA) as well as the PT, FI, PM, and NN models. The change in LE with changing T_a was greatest for TH, followed by HU and HA (Fig. 11). The change for PT, FI, and PM was marginal (8–10 W m^{-2}); the NN model decreased LE by 7 W m^{-2}. It is therefore critical to select an appropriate LE model when integrating it as a component to larger models of global change and prediction.

To summarize, we presented a rigorous evaluation of 13 LE models against the largest dataset of LE from tropical vegetation assembled to date – 21 tropical eddy covariance sites. We found that R_n was by far the strongest determinant of LE, and VPD was the strongest residual predictor, followed by NDVI, PPT, and u; T_a was not a strong residual predictor of tropical LE. The radiation-based models performed best overall for three reasons: (1) the vegetation was largely decoupled from the atmosphere, especially at the wetter sites; (2) the resistance-based models were hindered by difficulty in consistently characterizing r_c; (3) the temperature-based models inadequately captured the variability in tropical LE. We extrapolated a model of LE to a test region – Amazonia – and demonstrated that the asymmetric position of Amazonia relative to the equator most likely drives the spatial and seasonal variation of LE from this region. We estimated a mean region-wide LE of 1370 mm yr^{-1} based on one of the best performing models driven with data from the ISLSCP-II archive, but this value is critically dependent on the assumption that eddy covariance studies in the tropics produce more robust values of evaporative fraction rather than absolute LE – if the absolute values of LE from eddy covariance measurements are more accurate, the basin-wide LE would be closer to 1096 mm. This highlights an important issue in the use of flux data to validate and interpolate models: how do we manage the lack of energy balance closure in most field observations? Our answer to this question has important ramifications for our estimates of the evaporative flux of the land biosphere.

References

Alves I, Cameira MD (2002) Evapotranspiration estimation performance of root zone water quality model: evaluation and improvement. *Agricultural Water Management*, **57**, 61–73.

Araújo AC, Nobre AD, Kruijt B et al. (2002) Comparative measurements of carbon dioxide fluxes from two nearby towers in a central Amazonian rainforest: The Manaus LBA site. *Journal of Geophysical Research*, **107**, 8090–9091.

Aubinet M, Heinesch B, Yernaux M (2003) Horizontal and vertical CO$_2$ advection in a sloping forest. *Boundary-Layer Meteorology*, **108**, 397–417.

Baldocchi D, Falge E, Gu LH et al. (2001) FLUXNET: a new tool to study the temporal and spatial variability of ecosystem-scale carbon dioxide, water vapor, and energy flux densities. *Bulletin of the American Meteorological Society*, **82**, 2415–2434.

Baumgartner A, Reichel E (1975) *The World Water Balance*. Elsevier, New York, NY, USA.

Bigelow S (2001) Evapotranspiration modelled from stands of three broad-leaved tropical trees in Costa Rica. *Hydrological Processes*, **15**, 2779–2796.

Bonal D, Bosc A, Ponton S et al (in press) The impact of severe dry season on net ecosystem exchange in the Neotropical rainforest of French Guiana. *Global Change Biology*, **14**, 1917–1933.

Carswell FE, Costa AL, Palheta M et al. (2002) Seasonality in CO_2 and H_2O flux at an eastern Amazonian rain forest. *Journal of Geophysical Research – Atmospheres*, **107**, 8076–8092.

Costa MH, Foley JA (1997) The water balance of the Amazon Basin dependence on vegetation cover and canopy conductance. *Journal of Geophysical Research – Atmospheres*, **102**, 23973–23989.

Cox PM, Betts RA, Jones CD, Spall SA, Totterdell IJ (2000) Acceleration of global warming due to carbon-cycle feedbacks in a coupled climate model. *Nature*, **408**, 184–187.

da Rocha HR, Goulden ML, Miller SD, Menton MC, Pinto LDVO, de Freitas HC, Silva Figueira AME (2004) Seasonality of water and heat fluxes over a tropical forest in eastern Amazonia. *Ecological Applications*, **14**, S22–S32.

Epron D, Nouvellon Y, Roupsard O et al. (2004) Spatial and temporal variations of soil respiration in a Eucalyptus plantation in Congo. *Forest Ecology and Management*, **202**, 149–160.

Farahani HJ, Ahuja LR (1996) Evapotranspiration modeling of partial canopy/residue-covered fields. *Transactions of the American Society of Agricultural Engineers*, **39**, 2051–2064.

Finnigan JJ, Clement R, Malhi Y, Leuning R, Cleugh HA (2003) A re-evaluation of long-term flux measurement techniques – Part I: averaging and coordinate rotation. *Boundary-Layer Meteorology*, **107**, 1–48.

Fisher JB, Baldocchi DD, Misson L, Dawson TE, Goldstein AH (2007) What the towers don't see at night: nocturnal sap flow in trees and shrubs at two AmeriFlux sites in California. *Tree Physiology*, **27**, 597–610.

Fisher JB, Debiase TA, Qi Y, Xu M, Goldstein AH (2005) Evapotranspiration models compared on a Sierra Nevada forest ecosystem. *Environmental Modelling & Software*, **20**, 783–796.

Fisher JB, Tu K, Baldocchi DD (2008) Global estimates of the land–atmosphere water flux based on monthly AVHRR and ISLSCP-II data, validated at 16 FLUXNET sites. *Remote Sensing of Environment*, **112**, 901–919.

Goulden ML (1996) Carbon assimilation and water-use efficiency by neighboring Mediterranean-climate oaks that differ in water access. *Tree Physiology*, **16**, 417–424.

Goulden ML, Miller SD, da Rocha HR, Menton MC, de Freitas HC, Figueira AMES, de Sousa CAD (2004) Diel and seasonal patterns of tropical forest CO_2 exchange. *Ecological Applications*, **14**, S42–S54.

Grace J, Malhi Y, Higuchi N, Meir P (2001) Productivity of tropical forests. In: *Terrestrial Global Productivity* (eds Roy J, Saugier B, Mooney HA), pp. 401–426. Academic Press, San Diego, CA, USA.

Granier A, Huc R, Barigah ST (1996) Transpiration of natural rain forest and its dependence on climatic factors. *Agricultural and Forest Meteorology*, **78**, 19–29.

Grant RF (1998) Simulation in ecosys of root growth response to contrasting soil water and nitrogen. *Ecological Modelling*, **107**, 237–264.

Hall FG, Collatz GJ, Los SO, Brown E, Colstoun DE, Landis D (eds) (2005) *ISLSCP Initiative II: DVD/CD-ROM*, NASA.

Hamon WR (1963) Computation of direct runoff amounts from storm rainfall. *International Association of Scientific Hydrology Publication*, **63**, 52–62.

Hasler N, Avissar R (2007) What controls evapotranspiration in the Amazon Basin? *Journal of Hydrometeorology*, **8**, 380–395.

Hirano T, Segah H, Harada T, Limin S, June T, Hirata R, Osaki M (2007) Carbon dioxide balance of a tropical peat swamp forest in Kalimantan, Indonesia. *Global Change Biology*, **13**, 412–425.

Huete AR (1988) A soil-adjusted vegetation index (SAVI). *Remote Sensing of Environment*, **25**, 295–309.

Huete AR, Restrepo-Coupe N, Ratana P et al. (2008) Multiple site tower flux and remote sensing comparisons of tropical forest dynamics in Monsoon Asia. *Agricultural and Forest Meteorology*, **148**, 748–760.

Hulme M, Viner D (1998) A climate change scenario for the tropics. *Climatic Change*, **39**, 145–176.

Hutyra LR, Munger JW, Nobre CA, Saleska SR, Vieira SA, Wofsy SC (2005) Climatic variability and vegetation vulnerability in Amazônia. *Geophysical Research Letters*, **32**, 1–4.

Jarvis PG, McNaughton KG (1986) Stomatal control of transpiration: scaling up from leaf to region. *Advances in Ecological Research*, **15**, 1–49.

Jensen ME, Haise HR (1963) Estimating evapotranspiration from solar radiation. *Journal of the Irrigation and Drainage Division American Society of Civil Engineers*, **89**, 15–41.

Juárez RIN, Hodnett MG, Fu R, Goulden ML, von Randow C (2007) Control of dry season evapotranspiration over the Amazonian forest as inferred from observations at a Southern Amazon forest site. *Journal of Climate*, **20**, 2827–2839.

Kang SZ, Hu XT, Goodwin I, Jerie P (2002) Soil water distribution, water use, and yield response to partial root zone drying under a shallow groundwater table condition in a pear orchard. *Scientia Horticulturae*, **92**, 277–291.

Kelly MA, Randall DA (2001) A two-box model of a zonal atmospheric circulation in the tropics. *Journal of Climate*, **19**, 3944–3964.

Kruijt B, Elbers JA, von Randow C et al. (2004) The robustness of eddy correlation fluxes for Amazon rain forest conditions. *Ecological Applications*, **14**, S101–S113.

Kumagai T, Saitoh TM, Sato Y et al. (2005) Annual water balance and seasonality of evapotranspiration in a Bornean tropical rainforest. *Agricultural and Forest Meteorology*, **128**, 81–92.

Larson K, Hartmann DL, Klein SA (1999) The role of clouds, water vapor, circulation, and boundary layer structure in the sensitivity of the tropical climate. *Journal of Climate*, **12**, 2359–2374.

Loescher HW, Gholz HL, Jacobs JM, Oberbauer SF (2005) Energy dynamics and modeled evapotranspiration from a wet tropical forest in Costa Rica. *Journal of Hydrology*, **315**, 274–294.

Los SO, Collatz GJ, Malmstrom CM *et al.* (2000) A global 9-year biophysical land surface dataset from NOAA AVHRR data. *Journal of Hydrometeorology*, **1**, 183–199.

Malhi Y, McNaughton K, Von Randow C (2004) Low frequency atmospheric transport and surface flux measurements. In: *Handbook of Micrometeorology*, Vol. 29 (eds Lee X, Massman W, Law B), pp. 101–118. Springer Netherlands, Dordrecht, the Netherlands.

Malhi Y, Pegoraro E, Nobre AD, Pereira MGP, Grace J, Culf AD, Clement R (2002) Energy and water dynamics of a central Amazonian rain forest. *Journal of Geophysical Research – Atmospheres*, **107**, 8061–8078.

Malhi Y, Wright J (2004) Spatial patterns and recent trends in the climate of tropical rainforest regions. *Philosophical Transactions of the Royal Society of London*, **359**, 311–329.

McNaughton KG, Black TA (1973) A study of evapotranspiration from a Douglas fir forest using the energy balance approach. *Water Resources Research*, **9**, 1579–1590.

Nepstad DC, Decarvalho CR, Davidson EA *et al.* (1994) The role of deep roots in the hydrological and carbon cycles of Amazonian forests and pastures. *Nature*, **372**, 666–669.

New M, Hulme M, Jones P (2000) Representing twentieth-century space–time climate variability. Part II: Development of 1901–1996 monthly grids of terrestrial surface climate. *Journal of Climate*, **13**, 2217–2238.

Numaguti A (1993) Dynamics and energy balance of the Hadley circulation and the tropical precipitation zones: significance of the distribution of evaporation. *Journal of Atmospheric Science*, **50**, 1874–1887.

Penman HL (1948) Natural evaporation from open water, bare soil and grass. *Proceedings of the Royal Society of London Ser. A*, Vol. 193, pp. 120–146.

Penman-Monteith JL (1965) Evaporation and the environment. *Symposium of the Society of Exploratory Biology*, **19**, 205–234.

Pinker RT, Laszlo I (1992) Modeling surface solar irradiance for satellite applications on a global scale. *Journal of Applied Meteorology*, **31**, 194–211.

Priestley CHB, Taylor RJ (1972) On the assessment of surface heat flux and evaporation using large scale parameters. *Monthly Weather Review*, **100**, 81–92.

Raupach MR, Finnigan JJ (1988) 'Single-layer models of evaporation from plant canopies are incorrect but useful, whereas multilayer models are correct but useless': discuss. *Australian Journal of Plant Physiology*, **15**, 705–516.

Robock A, Vinnikov KY, Schlosser CA, Speranskaya NA, Xue YK (1995) Use of midlatitude soil-moisture and meteorological observations to validate soil-moisture simulations with biosphere and bucket models. *Journal of Climate*, **8**, 15–35.

Rossow WB, Walker AW, Beuschel DE, Roiter MD (1996) International Satellite Cloud Climatology Project (ISCCP): Documentation of new cloud data sets. *World Meteorological Organization*, 115.

Roupsard O, Bonnefond J-M, Irvine M *et al.* (2006) Partitioning energy and evapo-transpiration above and below a tropical palm canopy. *Agricultural and Forest Meteorology*, **139**, 252–268.

Sakai RK, Fitzjarrald DR, Moraes OLL *et al.* (2004) Land-use change effects on local energy, water, and carbon balances in an Amazonian agricultural field. *Global Change Biology*, **10**, 895–907.

Saleska SR, Didan K, Huete AR, da Rocha HR (2007) Amazon forests green-up during 2005 drought. *Science*, **318**, 612.

Saleska SR, Miller SD, Matross DM *et al.* (2003) Carbon in Amazon forests: unexpected seasonal fluxes and disturbance-induced losses. *Science*, **302**, 1554–1557.

Schubert S, Suarez M, Park CK, Moorthi S (1993) GCM simulations of intraseasonal variability in the Pacific North-American region. *Journal of the Atmospheric Sciences*, **50**, 1991–2007.

Schüttemeyer D, Schillings C, Moene AF, De Bruin HAR (2007) Satellite-based actual evapotranspiration over drying semiarid terrain in West Africa. *Journal of Applied Meteorology and Climatology*, **46**, 97–111.

Shuttleworth WJ (1988) Evaporation from Amazonian rainforest. *Philosophical Transactions of the Royal Society of London*, **B233**, 321–346.

Shuttleworth WJ (1989) Micrometeorology of temperate and tropical forests. *Philosophical Transactions of the Royal Society of London*, **B324**, 299–334.

Shuttleworth WJ, Gash JH, Lloyd CR *et al.* (1984) Eddy correlation measurements of energy partition for Amazonian forest. *Quarterly Journal of the Royal Meteorological Society*, **110**, 1143–1162.

Shuttleworth WJ, Wallace JS (1985) Evaporation from sparse crops – an energy combination theory. *Quarterly Journal of the Royal Meteorological Society*, **111**, 839–855.

Soares-Filho BS, Nepstad DC, Curran LM *et al.* (2006) Modelling conservation in the Amazon Basin. *Nature*, **440**, 520–523.

Sommer R, Sa TTD, Vielhauer K, de Araujo AC, Folster H, Vlek PLG (2002) Transpiration and canopy conductance of secondary vegetation in the eastern Amazon. *Agricultural and Forest Meteorology*, **112**, 103–121.

Stackhouse PW, Gupta SK, Cox SJ, Chiacchio M, Mikovitz JC (2000) The WCRP/GEWEX Surface Radiation Budget Project Release 2: an assessment of surface fluxes at 1 degree resolution. In: *IRS 2000: Current Problems in Atmospheric Radiation* (eds Smith WL, Timofeyev YM), pp. 24–29. International Radiation Symposium, St. Petersburg, Russia.

Tanaka K, Takizawa H, Tanaka N *et al.* (2003) Transpiration peak over a hill evergreen forest in northern Thailand in the late dry season: assessing the seasonal changes in evapotranspiration using a multilayer model. *Journal of Geophysical Research*, **108**, ACL4.1–ACL4.15.

Thornthwaite CW (1948) An approach toward a rational classification of climate. *Geographical Review*, **38**, 55–94.

Toda M, Nishida K, Ohte N, Tani M, Mushiake K (2002) Observations of energy fluxes and evapotranspiration over terrestrial complex land covers in the tropical monsoon environment. *Journal of the Meteorological Society of Japan*, **80**, 465–484.

Turc L (1961) Estimation of irrigation water requirements, potential evapotranspiration: a simple climatic formula evolved up to date. *Annals of Agronomy*, **12**, 13–49.

Twine TE, Kustas WP, Norman JM *et al.* (2000) Correcting eddy-covariance flux underestimates over a grassland. *Agricultural and Forest Meteorology*, **103**, 279–300.

von Randow C, Manzi AO, Kruijt B *et al.* (2004) Comparative measurements and seasonal variations in energy and carbon exchange over forest and pasture in South West Amazonia. *Theoretical and Applied Climatology*, **78**, 5–26.

Vourlitis GL, Priante N, Hayashi MMS, Nogueira JD, Caseiro FT, Campelo JH (2002) Seasonal variations in the evapotranspiration of a transitional tropical forest of Mato Grosso, Brazil. *Water Resources Research*, **38**, 30–41.

Werth D, Avissar R (2004) The regional evapotranspiration of the Amazon. *Journal of Hydrometeorology*, **5**, 100–109.

Williams M, Malhi Y, Nobre AD, Rastetter EB, Grace J, Pereira MGP (1998) Seasonal variation in net carbon exchange and evapotranspiration in a Brazilian rain forest: a modelling analysis. *Plant, Cell and Environment*, **21**, 953–968.

Wilson K, Goldstein A, Falge E *et al.* (2002) Energy balance closure at FLUXNET sites. *Agricultural and Forest Meteorology*, **113**, 223–243.